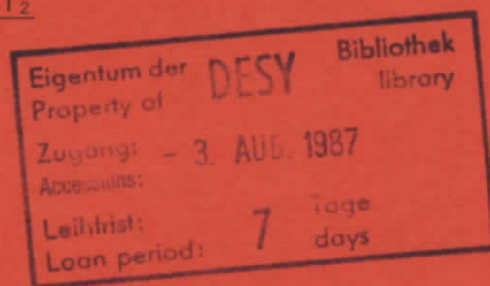


DESY SR 87-06
June 1987

ANALYSIS OF BOUND-FREE FLUORESCENCE AND IMPROVED CHARACTERIZATION
OF THE ELECTRONIC AND SPECTROSCOPIC PROPERTIES
OF THE $1\ \Sigma_u^+$ STATE OF Cl_2

by



J. Wörmer, T. Möller, J. Stapelfeldt, G. Zimmerer

II. Institut f. Experimentalphysik, Universität Hamburg

D. Haaks, S. Kampf

FB Physikalische Chemie, Universität GHS Wuppertal

J. Le Calvé

Centre d'Etudes Nucléaires de Saclay, IRDI, DESTCP

Département de Physico-Chimie, Gif-sur-Yvette

M.C. Castex

*Laboratoire des Interactions Moléculaires et des Hautes Pressions
du C.N.R.S., Centre Universitaire Paris-Nord, Villetaneuse*

ISSN 0723-7979

DESY behält sich alle Rechte für den Fall der Schutzrechtserteilung und für die wirtschaftliche Verwertung der in diesem Bericht enthaltenen Informationen vor.

DESY reserves all rights for commercial use of information included in this report, especially in case of filing application for or grant of patents.

To be sure that your preprints are promptly included in the
HIGH ENERGY PHYSICS INDEX,
send them to the following address (if possible by air mail):

**DESY
Bibliothek
Notkestrasse 85
2 Hamburg 52
Germany**

Analysis of Bound-Free Fluorescence and Improved Characterization
of the Electronic and Spectroscopic Properties
of the $1^1\Sigma_u^+$ State of Cl_2

J. Wörmer (a), T. Möller (a), J. Stapelfeldt (a), G. Zimmerer (a),
D. Haaks (b)*, S. Kampf (b), J. Le Calvé (c) and M.C. Castex (d)

- (a) II. Institut für Experimentalphysik, Universität Hamburg, Federal Republic of Germany
(b) FB Physikalische Chemie, Universität GHS Wuppertal, Federal Republic of Germany (*now at: Spectra-Physics GmbH, Darmstadt, Federal Republic of Germany)
(c) Centre d'Etudes Nucléaires de Saclay, IRDI, DESICP, Département de Physico-Chimie, Gif-sur-Yvette, France
(d) Laboratoire des Interactions Moléculaires et des Hautes Pressions du C.N.R.S., Centre Universitaire Paris-Nord, Villetaneuse, France

Abstract

Synchrotron radiation is used to selectively excite the chlorine molecule in the VUV spectral range. Stationary fluorescence spectra of the $1^1\Sigma_u^+$ state are observed following primary excitation of $1^1\Sigma_u^+$ and $2^1\Sigma_u^+$. The bound-free part of the spectra is analysed with the aid of quantum mechanical computer simulations. A potential energy curve is constructed which is an approximation of the adiabatic double well potential energy curve of the $1^1\Sigma_u^+$ state. The inner well is characterized by $T_e = (73428 \pm 50) \text{ cm}^{-1}$, $r_e = (1.85 \pm 0.05) \text{ \AA}$; for the outer well hold $T_e = (64631 \pm 50) \text{ cm}^{-1}$, $r_e = (2.57 \pm 0.05) \text{ \AA}$, $\omega_e = (261 \pm 5) \text{ cm}^{-1}$, $\omega_e x_e = (0.668 \pm 0.01) \text{ cm}^{-1}$ ($^{35}Cl_2$; $v' < 30$). The potential energy curve is successfully checked with fluorescence excitation spectra. Within the error limits, the results of a former synchrotron radiation study are verified. It is ruled out, that the Cl_2 "γ-state" recently observed with laser spectroscopic methods, can be attributed to the outer well of $1^1\Sigma_u^+$.

PACS: 3310; 3350; 3370

submitted to: Z. Phys. D: Atoms, Molecules and Clusters

1. Introduction

A few years ago, the electronic structure of the Cl_2 molecule in the vacuum ultraviolet (VUV) spectral range was known only in fragments [1]. Early absorption studies in the VUV yielded a lot of vibrational structure indicating the existence of bound excited states [2]. An unambiguous classification into different progressions together with the extraction of reliable potential energy curves was not possible. Early VUV fluorescence studies indicated a complex nature of the spectra [3] and enabled only a precise determination of the ground state [4,5].

In 1981, Peyerimhoff and Buenker performed the first ab initio calculations of the electronic structure of the Cl_2 molecule [6]. The results turned out to be an efficient tool for a better understanding of the electronic and spectroscopic properties of Cl_2 . The excited states potential energy curves present strong avoided crossings between Rydberg- and ion-pair (valence) states of the same symmetry which are responsible for irregularities in the optical spectra. Whereas in the first calculation spin-orbit interaction was not taken into account, this was done for a few selected states in the following paper [7]. Simultaneously, Douglas performed a high resolution absorption study in the spectral range between 145 and 120 nm [8]. From the rotational analysis of various progressions he was able to deduce the symmetry and the rotational constants of several excited states. Möller et al. [9] carried out a synchrotron radiation absorption and fluorescence experiment in the VUV. Taking into account the calculations [6] and the symmetry analysis of Douglas [8], they were able to assign several optically allowed transitions and to deduce the potential energy curves of some "ungerade" excited states. Jureta et al. [10] and Spence et al. [11] characterized some "gerade" states by low energy electron loss spectroscopy. Recently, Lee et al. extended the analysis of the optical spectra to the ionization limit [12].

Since 1981, Ishiwata et al. [13-17] and Shinzawa et al. [18] have undertaken a study of ion-pair excited states of halogens, in particular the gerade and ungerade spin-orbit components of the Cl_2 ion-pair states dissociating in the $Cl^+ ({}^3P \text{ or } {}^1D) + Cl^- ({}^1S)$ ionic limits. They use a sequential multiphoton optical optical double resonance (OODR) technique. With a first photon ($\lambda = 500 \text{ nm}$) a specific rovibronic level of the bound $B^3\Pi (0_u^+)$ state is reached. With a subsequent resonant two-photon absorption process (λ variable), three new Cl_2 $1^1\Sigma_u^+ (0_u^+)$ states were found by exploring the region of 60000 cm^{-1} [14]. The two lowest ones (the "α-state"



with $T_e = 58487 \text{ cm}^{-1}$ and the " β -state" with $T_e = 58587 \text{ cm}^{-1}$) were assigned to the two O_u^+ spin-orbit components of the $^3\Sigma_u^-$ (3P_2) and $2^3\Pi_u$ (3P_0) states.

The third one, called " γ -state", was attributed to the lowest ion-pair state with $^1\Sigma_u^+$ symmetry which is identical with the $1^1\Sigma_u^+$ state already characterized by Möller et al. [9]. Möller et al. found $T_e = 65227 \text{ cm}^{-1}$, in good agreement with the ab initio calculations [6]. The T_e value of the " γ -state", however, is 59926 cm^{-1} [14], in striking contrast to the result of Möller et al. [9]. Ishiwata et al. were aware of this problem. Indeed, Möller et al. were able to perform absorption and fluorescence excitation studies of the $1^1\Sigma_u^+$ state only for $v' > 30$ (in the Franck-Condon regime). The T_e value could not be extracted from the absorption and fluorescence excitation spectra but was estimated taking into account the results of the ab initio calculations [6] and preliminary bound-free fluorescence spectra, $1^1\Sigma_u^+ + x^1\Sigma_g^+$ [9]. Maybe, for this reason, Ishiwata et al. did not take seriously into consideration the discrepancy in the T_e values. Another not yet solved discrepancy between Ishiwata et al. [13,14] and Möller et al. [9] concerns the wavelength range of fluorescence of both states under discussion. Whereas Möller et al. [9] report on strong fluorescence around 200 nm, Ishiwata et al. [13] observed fluorescence around 235 nm.

It is the first aim of this paper to clarify the discrepancy between the results of Ishiwata et al. [14] and Möller et al. [9]. In order to be sensitive for the shape of the $1^1\Sigma_u^+$ potential energy curve around the minimum, in the present work the spectral shape of the bound-free fluorescence spectra was carefully studied. Anticipating the results it can be stated that within the error limits given in [9] the new results agree with the former ones. It can be excluded definitely that the γ -state is identical with the $1^1\Sigma_u^+$ state (the lowest ion-pair state with $^1\Sigma_u^+$ symmetry).

A strong avoided crossing between the first Rydberg and ion-pair Cl_2 state of $^1\Sigma_u^+$ symmetry gives rise to a double well shape of the $1^1\Sigma_u^+$ and an inner $2^1\Sigma_u^+$ adiabatic potential energy curve [6,9]. The fluorescence spectra presented in this paper were obtained following either

- (i) primary vibrationally selective excitation of the $1^1\Sigma_u^+$ outer well region,
- (ii) the region of the hump separating the inner from the outer well, and
- (iii) the $2^1\Sigma_u^+$ state, which dominates in optical absorption between 78000 cm^{-1} and 83000 cm^{-1} [9,12].

It is the second aim of this paper to get a deeper insight into the interaction of both states. For this purpose, the excitation energy was tuned through the large range indicated above (more than 20000 cm^{-1}). To the best of our knowledge, up to now only in the case of H_2 , the excitation energy was tuned over such an extended energy range in a study of bound-free fluorescence [19]. Both, in the beautiful experiment of Schmoranzner et al. [19] and in the present work, this was only possible making use of synchrotron radiation as an efficient VUV excitation source.

2. Experiment

The experiments were carried out on the SUPERLUMI beam line at HASYLAB. Primary excitation of Cl_2 was performed optically with synchrotron radiation between 66555 cm^{-1} and 87360 cm^{-1} . Spectral resolution was achieved with a 2m-normal incidence monochromator [20] with a resolution interval $\Delta\lambda$ between 0.01 nm and 0.25 nm. The spectral resolution was sufficiently high for vibrationally selective excitation of Cl_2 . However, it was not possible to discriminate completely between the different isotopic species ($^{35}Cl_2$, $^{35}Cl^{37}Cl$, $^{37}Cl_2$) because gas with natural abundance was used (Matheson research quality).

The pressure of Cl_2 in the gas cell with LiF windows was typically 0.1 Torr. In view of the short radiative lifetime of the electronic state under discussion ($^1\Sigma_u^+$, $\tau = 3 \text{ ns}$ [21]) this is already sufficient to guarantee collision free conditions. For the analysis of bound-bound fluorescence spectra which can be influenced by reabsorption, the pressure was lowered down to $\approx 10^{-2}$ Torr. Compared to our earlier experiment [9] this is a considerable improvement.

The fluorescence light was analyzed perpendicular to the exciting beam. The bound-free spectra were scanned with a spectral resolution interval of 1.0 nm with a high flux ($f/2.8$) VUV monochromator [22]. The bound-bound fluorescence spectra were analyzed with a 1m-VUV monochromator set in operation only recently [23]. In this way it was possible to work with a resolution interval of $\Delta\lambda \geq .08 \text{ nm}$. All experiments were carried out at room temperature.

Generally, the single photon counting method was used. Exploiting the time structure of synchrotron radiation (pulses with a FWHM of $\approx 130 \text{ ps}$ at a repetition rate of $\approx 1 \text{ MHz}$; numbers only valid for the storage ring DORIS

at Hamburg) it was possible to measure routinely the correlation of the fluorescence events to the excitation pulses. Though time-resolved results are not presented in this paper, this point has to be mentioned because it is the basis for an efficient suppression of the dark counting rate of the multiplier (solar blind type multiplier with MgF_2 window [Hamamatsu R 1460], Valvo XP 2020 Q). The suppression is achieved registering the signal only in a time window $\Delta t < 10 \tau$ ($\Delta t \ll$ repetition time!) immediately following the excitation pulses. The details are described in, e.g., [24]. The values of Δt are given in the figure captions.

3. Results and Discussion

3.1 General view of the fluorescence spectra and qualitative interpretation

In Fig. 1, two typical fluorescence spectra of 0.1 Torr Cl_2 are presented. The lower curve is obtained following primary excitation of $2 \ ^1\Sigma_u^+$ ($v' = 0$) ($E_{\text{ex}} = 78135 \text{ cm}^{-1}$) [9]. With the excitation energy of 73755 cm^{-1} (upper curve), in agreement with the rotational analysis of Douglas [8], a state with $^1\Sigma_u^+$ symmetry is reached ($^{35}\text{Cl}_2$). Möller et al. [9] assigned it to $v' = 39 \pm 2$ of the $1 \ ^1\Sigma_u^+$ state. As we shall see below, in view of the new results presented here, the vibrational quantum has to be changed to $v' = 41$.

In the fluorescence spectra two different parts can be distinguished

- (i) bound-bound fluorescence between E_{ex} and E_2 , and
- (ii) bound-free fluorescence between E_2 and the long wavelength onset of fluorescence.

The bound-bound fluorescence terminates at $X \ ^1\Sigma_g^+$ (v''). Due to the medium spectral resolution, the vibrational quanta of the ground state are not all clearly resolved. The beats in the intensities (upper curve) are due to the fact that the vibrational quantum of the ground state is roughly twice as large as that of the excited state. Though the bound-bound part of the fluorescence spectra is not a central aspect of this paper, we present one example of our results obtained with a better spectral resolution (Fig. 2). The excitation energy, $E_{\text{ex}} = 73448 \text{ cm}^{-1}$ corresponds to $1 \ ^1\Sigma_u^+$ ($v' = 39$) + $X \ ^1\Sigma_g^+$ ($v'' = 0$) (Möller et al. [9] assigned it to $v' = 37$). The maxima of the spectrum of Fig. 2 reflect the vibrational spacing of the ground state. For comparison purposes, the $1 \ ^1\Sigma_u^+$ ($v' = 39$) + $X \ ^1\Sigma_g^+$ (v'') transition energies were calculated from the potential energy parameters of the ground

state [5] and the excitation energy. They are indicated in the figure by bars.

Möller et al. [9] already showed that the longer wavelength part of the spectra is due to $1 \ ^1\Sigma_u^+ + X \ ^1\Sigma_g^+$ bound-free emission. The bound-free nature and the special role of the energetic positions E_2 and E_3 indicated in Fig. 1 are explained in Fig. 3. Here we present the potential energy curves of the Cl_2 ground state and of the emitting double well state. Included is the difference potential (dotted line). Suppose that the vibrational level of the excited state indicated by a line was selectively excited. Then the high energy onset of fluorescence is emitted at $E_0 = E_{\text{ex}}$, terminating at the zeroth vibrational level of the ground state. According to the classical Franck-Condon principle, the fluorescence transitions represented by vertical arrows, terminate at the difference potential. Therefore the fluorescence spectrum extends from E_{ex} to E_3 which corresponds to a transition terminating at the top of the difference potential. The energy E_2 is the onset of bound-free transitions, all arrows between E_2 and E_3 terminating in the continuum of the ground state. From the figure it is immediately clear that E_0 and E_2 shift linearly with the excitation energy E_{ex} , see also Fig. 1. In the classical Franck-Condon approximation, however, E_3 is independent from the excitation energy.

A careful inspection of the upper curve of Fig. 1 shows that the energy E_2 does not necessarily coincide with the qualitative change of the shape of the fluorescence spectra from the bound-bound to the bound-free part. This change is better described by an energy E_1 , which is explained in Fig. 3. It represents the energy of the transition terminating at the difference potential where it crosses the ground state. Transitions between E_1 and E_2 still terminate at bound states, however, the main contribution stems from an internuclear distance at which the kinetic energy is nearly zero which leads to an enhancement of the FC-factors. The vibrational spacing of the ground state near to the dissociation limit is not resolved in the curves of Fig. 1. Therefore, the long-wavelength end of bound-bound transitions looks already more or less like bound-free transitions. With increasing excitation energy, E_1 more and more approaches E_2 . This is immediately clear from Fig. 3.

Taking into account the quantum mechanical description [25] instead of the classical Franck-Condon principle, it is well known that the FC-parameters for bound-free fluorescence transitions include two types of interference effects, namely a coarse structure and a fine structure. This

has been described in detail, e.g., by Tellinghuisen [26]. It turns out, that the position of the low energy maximum of the coarse structure **approximately** coincides with E_3 [27]. The fluorescence in this part of the spectrum is pronounced because the molecule can radiate into the same interval of photon energy at a relatively large fraction of the internuclear distance. The position of the low energy maximum of the coarse structure shifts only slightly with increasing excitation energy. All these features which are predicted by theory, can be observed in our results (see also below). Therefore the bound-free nature of the fluorescence between E_2 and E_3 is well established.

3.2 Computer simulation of the bound-free spectra and the potential energy curve of the $1^1\Sigma_u^+$ state

For the computer simulations of the bound-free spectra, the ground state parameters of Table 1 were taken. The potential energy curve was approximated with a Hulbert-Hirschfelder potential [28]. Concerning the $1^1\Sigma_u^+$ state it was tried to find an analytical expression describing the double-well potential with the following requirements,

- (i) it should coincide with the inner-well part of the potential given by Möller et al. [9] because this was already determined with an accuracy sufficient for the purpose of this paper. Of course, the analytical expression also had to describe correctly the known asymptotic behaviour ($r \rightarrow \infty$);
- (ii) it should be constructed from two parts describing the Rydberg and the valence part in a physically significant way. The r-dependent weight functions (r: internuclear distance) should provide for a continuous merging of both parts one into each other in the center of the perturbation.

The latter point is especially mentioned, because the $2^1\Sigma_u^+$ state which has the same precursors as the $1^1\Sigma_u^+$ state was approximated with the same functions (more rigorously speaking: the inner minimum of $2^1\Sigma_u^+$). The details of the analytical expressions of the $1^1\Sigma_u^+$ potential energy curve are given in the appendix.

With the potential energy curves just described, the Franck-Condon overlap integrals for the bound-free transitions were calculated. For the simulation of the spectra we took into account additionally

- (i) the r-dependence of the transition moment,
- (ii) the density of final states,
- (iii) the $(h\nu)^4$ -dependence for fluorescence transitions.

The r-dependence was approximated by an interpolation of the theoretical values [6] and an extrapolation to larger r. Here, of course, is a source of error, but mainly for the variation of the relative intensities of the spectra.

The number of (equidistant) final states was 250. This corresponds to a spacing of the kinetic energy between two adjacent states by 5...15 meV. The density of final states was approximated by the density of states of a square well potential with high barriers and introduced into the calculation via weight functions.

The results were finally convoluted with the experimental apparatus function. Then the simulations were compared with the experiment. The parameters of the potential energy curve were changed until a satisfactory agreement between simulation and experiment was reached. For each change of a parameter, the potential energy curve had to be reconstructed in such a way that its well established parts were reproduced again.

It may be admitted to present the final results of the $1^1\Sigma_u^+$ potential energy curve before comparing the simulations with the experimental spectra. In Fig. 4, the final result for $1^1\Sigma_u^+$ is presented, together with the earlier result of Möller et al. [9] and the theoretical results obtained by Peyerimhoff and Buenker [6] and by Jaffee [29]. Jaffee only calculated the potential energy curves of the ion-pair states. Therefore a comparison is only possible for the outer well. The γ -state described by Ishiwata et al. [14] is included, too. More precisely speaking, the curve of the γ -state is a Morse potential energy curve which was calculated from the parameters of the γ -state. The new $1^1\Sigma_u^+$ curve and the former results of Möller et al. agree within the error limits. In the ionic part of the potential energy curves, good agreement with theory is achieved. The slight discrepancies between theory and experiment at smaller internuclear distances were already discussed by Möller et al. [9]. The discrepancy between the $1^1\Sigma_u^+$ state and the γ -state could not be removed. It is clear now, that the γ -state has to be ascribed to another electronic state of Cl_2 (see below). The new parameters which characterize the outer well of the $1^1\Sigma_u^+$ state are included in Table 1 and compared with the former ones [9]. The T_e and r_e value of the inner well were also added in Table 1 though they were

taken from [9]. However, in Fig. 5 of Ref. 9, the energy scale was shifted erroneously so that there was a source of ambiguity which is removed here-with.

3.3 Comparison between experimental and simulated spectra (outer well) and discussion of fluorescence excitation spectra

First of all, we compare measured and simulated spectra for primary excitation of outer well states below the inner well minimum. In this case, the potential energy curve is more or less unaffected by the interaction with the Rydberg state and good results can be obtained concerning the valence part of $1^1\Sigma_u^+$.

Bound-free fluorescence spectra following primary excitation of $1^1\Sigma_u^+$, $v' = 31, 36,$ and 37 are shown in Fig. 5, together with the simulated spectra (lower curves). In each case, good agreement is found between theory and experiment. The fourth curve (expanded wavelength scale) is a computer simulation with an analytical model (flat ground state at r_e of the excited state, harmonic excited state [27]). It can be compared only qualitatively with the measured curves because the Cl_2 molecule does not fulfill sufficiently well the conditions of the analytical model. It was added, however, because it visualizes the coarse and the fine structure.

The splitting between the fine structure oscillations is a sensitive measure of the equilibrium distance r_e of the excited state potential energy curve. The fine structure positions in the simulations develop in full accordance with the measurements. This proves that the errors estimated for such simulations are small (see Table 1). It was tried to shift r_e over a large range of r . It is possible to fit the coarse structure also for other r_e values (2.5-2.7 Å). Then, however, the fits get drastically worse for the fine structure. Indeed, the long-wavelength onset of bound-free transitions is a sensitive function of the excited state potential energy curve around the minimum. Summing up, a new potential energy curve for the $1^1\Sigma_u^+$ state was deduced which describes well the bound-free fluorescence from the outer well minimum. Moreover, it yields the correct asymptotic limit ($r \rightarrow \infty$) and in the range of the inner minimum it is identical with the former result of Möller et al. [9].

The validity of the new result can be checked with measurements of fluorescence excitation spectra. Results are shown in Fig. 6. In the upper curve, the total fluorescence was measured as a function of the excitation

energy, in the lower one only bound-free fluorescence at 200 nm (corresponding roughly to E_3). The vibrational levels calculated from the $1^1\Sigma_u^+$ potential energy curve are included (only for $^{35}\text{Cl}_2$). There is a clear and close 1:1 correspondence to the strongest excitation peaks. Moreover, there is good agreement with the bandhead energies of $^{35}\text{Cl}_2$ excitation with $1^1\Sigma_u^+$ symmetry analysed by Douglas [8]. Most of the remaining peaks can be ascribed to $^{35}\text{Cl}^{37}\text{Cl}$ and $^{37}\text{Cl}_2$.

The former $1^1\Sigma_u^+$ potential energy curve [9] was obtained from the excitation spectra only. An uncertainty for v' of ± 2 was given because the bottom of the outer well was only estimated. Now, additionally, the spectral shape of that part of fluorescence was included as a source of information, which is sensitive for the minimum. As a result, the T_e value has to be changed from 65227 cm^{-1} [9] to 64631 cm^{-1} (Table 1) leading to a change in the numbering of the vibrational levels by 2. The agreement between the calculated and the measured excitation peaks is now even better than in the earlier work [9].

The upper curve of Fig. 6 contains bound-free and bound-bound fluorescence, the lower one contains **bound-free fluorescence only**. The most striking difference between both curves is the intensity of $v' = 39$. To get more insight into this peculiarity, the intensity ratio of both types of emission was deduced from the fluorescence spectra as a function of vibrational quantum number and is plotted in Fig. 7. In the whole range it is about 1.5 ... 2 with one singular exception. For $v' = 39$ it is about 5. A similar result was also obtained by Lee et al. [12] who measured the excitation spectra of "VUV" and "UV" fluorescence of Cl_2 . The curve for "VUV" fluorescence yields an enhancement of $v' = 39$ at 136.1 nm in qualitative accordance with Fig. 6.

The peculiar behaviour of $v' = 39$ underlines once more the validity of the $1^1\Sigma_u^+$ potential energy curve. We have calculated the wavefunctions for the various vibrational levels and it turns out that $v' = 39$ is the only one localized in the inner well. Already Möller et al. [9] pointed out this peculiarity (in their work it was $v' = 37$). The overwhelming amount of bound-bound emission of $v' = 39$ (see also Fig. 2) is a clear proof of its localization in the inner well.

3.4 Bound-free fluorescence following primary excitation in the energy range of Rydberg-valence interaction

In Fig. 8, fluorescence spectra are presented for excitation energies between 73448 cm^{-1} and 86067 cm^{-1} . The experimental conditions were the same as with the measurements described in Sec. 3.3. The excitation energies are characterized by vibrational quantum numbers v_1' and v_2' . v_1' is the quantum number of the $1 \ ^1\Sigma_u^+$ double well state, v_2' of the $2 \ ^1\Sigma_u^+$ state (both $^{35}\text{Cl}^{37}\text{Cl}$). In parenthesis the quantum numbers for $^{35}\text{Cl}^{37}\text{Cl}$ which are accessible within the resolution interval are included.

The most striking feature is the fact that the overall shape of the long wavelength part of fluorescence is very similar to the outer well $1 \ ^1\Sigma_u^+$ bound-free fluorescence described in Sec. 3.3. The center of the long-wavelength part of the envelope agrees with the transition energy E_3 explained in Fig. 3. The measured spectra are compared with model calculations in which the $1 \ ^1\Sigma_u^+$ potential energy curve (see Sec. 3.3) was taken as an emitting state.

The comparison yields two main features:

- (i) In the long-wavelength part ($\approx 190 \text{ nm} - 210 \text{ nm}$), the shape of the fluorescence spectra is well reproduced.
- (ii) The high energy onset of bound-free fluorescence agrees with energy E_2 (except for the highest excitation energy).

Obviously, we observe bound-free fluorescence of the $1 \ ^1\Sigma_u^+$ state also under high energy excitation conditions. The potential energy curves deduced in Sec. 3.3 describe well the fluorescence spectra which are emitted in the vicinity of r_e of the outer well. Note, for the highest excitation energies involved, the kinetic energy of the molecule at r_e is of the order to 3 eV. Nevertheless, the bound-free oscillations are a sensitive function of the potential energy curve around the minimum.

The bound-free fluorescence onset at E_2 is at least partly sensitive for the shape of the potential energy curve at large internuclear distances, i.e. in that part which corresponds to the asymptotic limit. The good agreement of experiment and model calculation reflects the fact that this asymptotic limit is well described by the potential energy curve deduced in Sec. 3.3. For the highest excitation energies used, the agreement between the calculation and the experimental spectra is no longer good ($\lambda < 180 \text{ nm}$). This will be discussed at the end of the next section.

3.5 Validity of the $1 \ ^1\Sigma_u^+$ and the $2 \ ^1\Sigma_u^+$ potential energy curves and crossing of the gap

In the previous section, the primary excitation energies were characterized by vibrational quantum numbers of the $1 \ ^1\Sigma_u^+$ double well state and of the $2 \ ^1\Sigma_u^+$ state analysed by Möller et al. [9]. It was tried to explain the main features of bound-free fluorescence in terms of the $1 \ ^1\Sigma_u^+$ potential energy curve. The validity of this procedure has to be discussed critically.

The crossing of two potential energy curves of the same symmetry is forbidden, because the states interact one with each other [30]. This leads to avoided crossings. Concerning the Cl_2 states under discussion, an ionic type valence state with the electronic configuration $\sigma_g^1 \pi_u^4 \pi_g^4 \sigma_u^1$, and a Rydberg state, $\sigma_g^2 \pi_u^4 \pi_g^3 \sigma_u^1 4p\pi$ [6] with $1 \ ^1\Sigma_u^+$ (0_u^+) symmetry yield such a behaviour. The corresponding diabatic wavefunctions are Ψ ($1 \ ^1\Sigma_u^+$ Rydb.) and Ψ ($1 \ ^1\Sigma_u^+$ Val.).

Introducing now the interaction of the diabatic states leads to new, adiabatic wavefunctions Ψ ($1 \ ^1\Sigma_u^+$) and Ψ ($2 \ ^1\Sigma_u^+$). The nomenclature is taken in accordance with Ref. [6]. The situation is visualized in Fig. 9. The potential energy curve of Ψ ($1 \ ^1\Sigma_u^+$) has a double well structure. The potential energy curve of Ψ ($2 \ ^1\Sigma_u^+$) is much narrower than those of the diabatic precursors. Both curves are separated by a gap $\Delta E = 2W_{12}$. W_{12} is the matrix element of the operator, W , describing the interaction,

$$W_{12} = \langle \Psi^* (1 \ ^1\Sigma_u^+ \text{ Ryd.}) W \Psi (1 \ ^1\Sigma_u^+ \text{ Val.}) \rangle \quad (1)$$

According to the ab initio calculations [6], for the Cl_2 states under discussion, $\Delta E = 1800 \text{ cm}^{-1}$. However, neither the diabatic, nor the adiabatic states describe the motion of the nuclei correctly due to the inertia of the electrons.

The vibrational states can be described either in the basis of the nuclear-momentum coupled adiabatic states or in the basis of electronically coupled diabatic states [31],

$$\chi = a_1 \chi_{\text{Val}}^d (1 \ ^1\Sigma_u^+) + a_2 \chi_{\text{Ryd}}^d (1 \ ^1\Sigma_u^+), \quad (2a)$$

or

$$\chi = b_1 \chi_1^a (1 \ ^1\Sigma_u^+) + b_2 \chi_2^a (2 \ ^1\Sigma_u^+) \quad (2b)$$

Here $a_1 \dots b_2$ are the respective mixing coefficients, and χ means the respective wavefunction describing the nuclear motion. In principle, equations (2a) and (2b) should contain summations over different vibrational levels.

A rigorous treatment of experimental data therefore requires a deduction of χ which has to be disentangled according to equ. (2) in order to deduce the basis wavefunctions and the mixing coefficients. From the basis wavefunctions one then can try to deduce either the diabatic or the adiabatic potential energy curves.

In contrast to this procedure we chose an empirical method to describe the experimental results. An effective potential energy curve was constructed which yields the characteristics of the adiabatic state $\Psi (1 \ ^1\Sigma_u^+)$ namely the hump separating the inner well from the outer well. The effective potential energy curve was chosen in a way that the eigenvalues and the wavefunctions χ reproduce correctly (i) the energetic positions of the irregularly spaced excitations and (ii) the main features of fluorescence.

Strictly speaking, it would be wrong to classify the effective potential energy curve as "adiabatic". However, at least in certain limited ranges it seems to be a good approximation. E.g., this is true around the outer minimum, because there is definitely no energetical overlap of the diabatic precursors. Then, of course, the diabatic and the adiabatic curves coincide.

In the range of the gap, it is an experimental result, that the effective potential energy curve reproduces with deviations of less than 0.1% (typically 0.05 ... 0.01%) the energy eigenvalues. In our opinion this indicates that the coefficient b_1 in the representation of equ. (2b) dominates here against b_2 and that the empirically deduced potential energy curve is a good approximation of the adiabatic one.

The good agreement between experiment and model calculation is astonishing from another point of view. In the energy range of the double well there exist two other states which can interact with $1 \ ^1\Sigma_u^+$, namely a $3 \ ^1\Sigma_u^-$ state with its O_u^+ component and a $3 \ ^1\Pi_u$ state with its O_u^+ component [6]. Indeed, the $1 \ ^1\Sigma_u^+$ vibronic progression is slightly irregular even in the

outer well region. The model calculations did not take into account this additional perturbation.

For energies above 78000 cm^{-1} it is a striking experimental fact [9] that the absorption is governed by a slightly irregular vibrational progression with FC factors exceeding those of the other absorption features by about one order of magnitude. In the earlier work [9], this progression was empirically described by $T_g = 77894 \text{ cm}^{-1}$, $\omega_g = 1040 \text{ cm}^{-1}$, $\omega_g x_g = 42 \text{ cm}^{-1}$. The parameters were ascribed to the adiabatic $2 \ ^1\Sigma_u^+$ state (see Fig. 9). Here, again, it must be admitted that this is not correct in a rigorous sense. But in view of the dominant nature of the progression, the procedure may be justified as an approximation.

Concerning the validity of the repulsive part of the $1 \ ^1\Sigma_u^+$ potential energy curve in the energy range where it overlaps with $2 \ ^1\Sigma_u^+$, we have to admit that it is more or less an extrapolation from the well established part. Therefore, the quantum numbers v'_1 given in Fig. 8 should not be taken too serious above $v'_1 = 43$. As already pointed out, the agreement of measured and calculated bound-free oscillations between E_2 and $\approx 180 \text{ nm}$ is not good. The emission in this wavelength range is sensitive to the wavefunction at short internuclear distances which seem to be not well reproduced by the potential energy curve. Note, however, that the main purpose of the paper was the deduction of the potential energy curve below the $2 \ ^1\Sigma_u^+$ state, not above. Therefore this question is left open.

Next we discuss how the emitting $1 \ ^1\Sigma_u^+$ state is populated following primary excitation of $2 \ ^1\Sigma_u^+$. This is ascribed to a diabatic crossing of the gap between both potential energy curves. The probability of diabatic crossing is given by [30,32]

$$P_d(r_x) = e^{-\gamma} \quad (3)$$

with

$$\gamma = 4\pi^2 \cdot (W_{12}(r_x))^2 / (h \cdot v_{\text{rel}} \cdot \Delta F) \quad (4)$$

v_{rel} is the relative velocity of the nuclei at the internuclear position, r_x , of the gap, and ΔF is the difference of the gradients of the diabatic potential energy curves at r_x .

The probability was estimated by Möller [33]. Even for the lowest vibrational level of $2 \ ^1\Sigma_u^+$, it is of the order of .1 and increases rapidly with increasing vibrational quantum number. Therefore the observation of fluorescence from $1 \ ^1\Sigma_u^+$ has a quite natural explanation. These findings are in good agreement with calculations of Dressler [31], which predict these states to be an intermediate case between diabatic and adiabatic description.

At the end of this section we comment on the curve with the highest excitation energy of Fig. 8. In this spectrum, it is not possible to distinguish between bound-bound and bound-free emission. The excitation energy is so high that a second range of perturbation is reached. Here the potential energy curve of $\Psi \ (^1\Sigma_u^+ \text{ Ryd})$ crosses another ionic curve (see Fig. 9). On the basis of the data presently available it seems to be impossible to disentangle the influence of three interacting states. Nevertheless it is remarkable that the general shape of bound-free fluorescence around E_3 persists also under these extreme excitation conditions.

3.6 Coarse structure spacing as a function of excitation energy.

For a flat ground state and a harmonic excited state, the bound-free fluorescence spectra can be described analytically. This has been shown by e.g. Mies and Julienne [27]. Concerning the emission from the outer well of $1 \ ^1\Sigma_u^+$, the ground state is still not flat enough to take the analytical description of the bound-free spectra seriously into consideration. Nevertheless, Möller [33] tried to deduce a simple rule for the spacing of the coarse structure maxima from the analytical expressions of Mies and Julienne. The spacing, ΔE , is indicated in Fig. 5. Möller showed that ΔE should scale roughly as

$$\Delta E^3 \propto [E_{\text{ex}} - E_{\text{onset}}] \quad (5)$$

Here E_{ex} means the excitation energy, and E_{onset} is the excitation energy for which bound-free emission starts to occur. (In Fig. 3 we could construct the case of $E_{\text{ex}} = E_{\text{onset}}$ if the difference potential just touches the dissociation limit of the ground state.)

In Fig. 10, ΔE^3 is plotted as a function of the excitation energy. Except from the highest excitation energies, the measured points nicely fit relation (5). The intersection of the straight line with the abscissa

yields an onset energy of 67400 cm^{-1} . This is in rough agreement with the value of 69400 cm^{-1} deduced from the $1 \ ^1\Sigma_u^+$ and the $X \ ^1\Sigma_g^+$ potential energy curves. Regarding equ. (5) as a linear approximation for ΔE^3 as a function of $(E_{\text{ex}} - E_{\text{onset}})$ inspired us to include higher order terms. Indeed, inclusion of terms up to the third order results in a much better fit (dashed curve) which yields an onset energy of 69870 cm^{-1} in very good agreement with 69400 cm^{-1} .

The empirical result of Fig. 10 at least underlines once more that the emission under discussion (long-wavelength onset of the bound-free spectra) stems from the same electronically excited state. This is another support for our interpretation.

The gap between the two groups of points in Fig. 10 indicates that for this range of excitation no fluorescence measurements were performed. Indeed, between $\approx 75000 \text{ cm}^{-1}$ and 80000 cm^{-1} the absorption of Cl_2 is governed by $1 \ ^1\Pi_u + X \ ^1\Sigma_g^+$ transitions [9] which have a much higher oscillator strength than the weak $1 \ ^1\Sigma_u^+ + X \ ^1\Sigma_g^+$ transitions.

3.7 Bound-free fluorescence of $1 \ ^1\Sigma_u^+$ with excitation energies around 67000 cm^{-1}

In Fig. 11, the long-wavelength part of $1 \ ^1\Sigma_u^+$ fluorescence spectra is presented for low excitation energies. Due to the weak absorption, the measurements were performed at higher Cl_2 pressures. The curves with $E_{\text{ex}} = 68033 \text{ cm}^{-1}$ and 66555 cm^{-1} , e.g., were obtained with $p = 10$ torr. For the lowest excitation energies, the FC factors for $1 \ ^1\Sigma_u^+ \leftarrow X \ ^1\Sigma_g^+$ ($v'' = 0$) are negligibly small. Therefore, this type of excitation has to be ascribed to hot bands. This is plausible, because at $p = 10$ torr and at room temperature, the partial pressure of $v'' = 1$ molecules is 0.6 torr, for $v'' = 2$ molecules it is 0.04 torr.

At first sight, all of the spectra of Fig. 11 seem to display bound-free fluorescence around 200 nm. On the other side, in the previous section it was shown, that $1 \ ^1\Sigma_u^+$ bound-free emission requires an excitation energy of at least 69400 cm^{-1} (starting from $v'' = 0$). Hot bands cannot account for the difference between 69400 cm^{-1} and, e.g., 66555 cm^{-1} , because at room temperature the thermal population of vibrational levels $\approx 3000 \text{ cm}^{-1}$ above $v'' = 0$ is really negligibly small. The explanation of the fluorescence

spectrum with $E_{\text{ex}} = 66555 \text{ cm}^{-1}$, e.g., might then appear puzzling with respect to our results concerning the potential energy curves of $1^1\Sigma_u^+$.

The problem could be solved taking into account a result of a recent fluorescence study on Cl_2 performed by Yu [34]. The curve he obtained with $E_{\text{ex}} = 68027 \text{ cm}^{-1}$ at $p = 10$ torr is reproduced separately in Fig. 12. The spectral resolution was sufficiently high to yield more details than we could detect. All the details of the spectrum can be explained by bound-bound transitions. The excitation (68027 cm^{-1}) obviously starts from $v'' = 1$ and terminates at $1^1\Sigma_u^+$ ($v' = 16$). Under this assumption, the transition energies for bound-bound transitions to $v'' = 37 \dots 49$ were calculated and the corresponding wavelengths are included in Fig. 12. They coincide with measured peaks or shoulders. One peak between $v' = 40$ and 41 is left. It may be due to primary excitation from $v'' = 2$ to $v' = 19$. The fluorescence transition back to $v'' = 43$ then agrees with the peak.

Summing up, the observation of fluorescence around 200 nm following primary excitation with low excitation energies is not in contradiction but corroborates the $1^1\Sigma_u^+$ potential energy curve. Only the type of fluorescence changes from bound-free to bound-bound.

3.8 A new interpretation of the " γ -state"

The results presented so far definitely rule out that the " γ -state" observed by Ishiwaka et al. [14] can be ascribed to $1^1\Sigma_u^+$. In Fig. 13 we present again the potential energy curves under discussion. Included are now recent results of an ab initio calculation of the $2^3\Pi_u$ state terminating at $\text{Cl}^+ (^3P_0) + \text{Cl}^-$ [35]. This state has a O_u^+ component. The very good agreement between the calculated curve and the " γ -state" curve strongly supports the assignment of the γ -state to the O_u^+ component of $2^3\Pi_u$.

Then, however, the question arises, how to interpret the α - and the β -state which both have O_u^+ symmetry [14]. In the complete analysis of existing states for the electronic configurations under discussion performed by Lee and Walsh [2], there is left only one candidate with the correct symmetry, namely the lowest $3^3\Sigma_u^-$ state which has a O_u^+ and a 1_u component. The O_u^+ component could account for either the α - or the β -state, but not for both. One could speculate about a heterogeneous interaction of the O_u^+ and the 1_u component, each of them having some O_u^+ character. In the case of Br_2 , this type of interaction has been characterized [36,37].

However, for a heterogeneous interaction, a strong dependence on the rotational quantum number is expected in contrast to the nearly regular patterns observed by Ishiwata et al. [14]. The open problem will have to be addressed in future work as has been pointed out by Tellinghuisen and Chakraborty [38].

4. Concluding Remarks

Though the Cl_2 molecule is one among the few diatomic molecules which exist under normal conditions in nature, its electronic structure in the VUV spectral range could be successfully attacked only in recent years with different methods. The present paper presents precise data on the $1^1\Sigma_u^+$ state which is of special importance because of its double well structure which originates from the interaction of a Rydberg- and a valence state. It was shown that the center of this interaction is within the Franck-Condon region. Therefore, Cl_2 may serve as a model for this type of molecular dynamics. The $1^1\Sigma_u^+$ state is also of interest from another point of view. Recently, e.g., it has been identified as a precursor state in elementary reactions of excited Cl_2 with Ar atoms leading to the formation of ArCl molecules [39].

The results presented in this paper rule out some severe discrepancies concerning the $1^1\Sigma_u^+$ state published in recent years. Nevertheless, the state of the art concerning the understanding is not satisfactory for the following reasons:

- (i) It was not possible up to now to deduce the true adiabatic (or diabatic) potential energy curves from the experimental spectra but only approximations (which may be rather near to the true adiabatic state).
- (ii) Still, the interaction of all diabatic states of O_u^+ symmetry is not fully taken into account. The irregularities of the $1^1\Sigma_u^+$ progression in the outer well, e.g., deserve further experimental investigations.

The work presented here was performed with vibrationally selective excitation in the VUV spectral range. A further improvement could be achieved if rotationally selective excitation could be used in the fluorescence experiments. With the present experimental limitations in connection with synchrotron radiation this is not feasible. However, it seems to us that high resolution laser excitation could push forward our knowledge on the electronic structure of Cl_2 considerably.

Acknowledgement

The authors wish to thank Prof. D.W. Setser who brought to their attention the thesis work of Dr. Yu. The support by the staff of HASYLAB is gratefully acknowledged. Finally we wish to thank Prof. S.D. Peyerimhoff, who made us available new results prior to publication. This work has been funded by the German Federal Minister for Research and Technology (BMFT) under the contract number 05 305 AXBO TP7.

Table 1

Parameters of the Hulbert-Hirschfelder approximation of the ground state of Cl_2 , deduced from [5], and parameters of the outer well and of the inner well of the $1^1\Sigma_u^+$ state.

$X^1\Sigma_g^+$

$$V(r) = D_e [(1 - e^{-x})^2 + C x^3 e^{-2x} (1 + bx)], \quad x = 2\beta[(r - r_0)/r_0]$$

$$D_e = 20277 \text{ cm}^{-1}$$

$$\beta = 1.989$$

$$r_0 = 1.988 \text{ \AA}$$

$$C = 0.2126$$

$$b = 1.2121$$

$1^1\Sigma_u^+$ (outer minimum, $^{35}\text{Cl}_2$)

T_e/cm^{-1}	$r_e/\text{\AA}$	ω_e/cm^{-1}	$\omega_e x_e/\text{cm}^{-1}$	Reference
64631 ± 50	2.57 ± 0.05	261 ± 5	0.668 ± 0.01	this work
65400	2.69			[29]
65300 ± 800	2.71 ± 0.03	225 ± 25		[6]
65227	2.62	243	0.33	[9]
59926	2.94	282.9	2.18	[14]

$1^1\Sigma_u^+$ (inner minimum)

73428 ± 50	1.85 ± 0.05			this work
73428	1.852			[9]

References

- 1 K.P. Huber and G. Herzberg, Molecular spectra and molecular structure, Vol. 4. Constants of diatomic molecules (Van Nostrand, Princeton, 1979), and references therein.
- 2 J. Lee and A.D. Walsh, Trans. Faraday Soc. 55, 1281 (1959)
- 3 R.K. Asundi and P. Venkateswarlu, Indian J. Phys. 21, 76 (1947); P. Venkateswarlu, Proc. Indian Acad. Sci. A26, 22 (1947)
- 4 Y.V. Rao and P. Venkateswarlu, J. Mol. Spectrosc. 9, 173 (1962)
- 5 A.E. Douglas and A.R. Hoy, Can. J. Phys. 53, 1965 (1975)
- 6 S.D. Peyerimhoff and R.J. Buenker, Chem. Phys. 57, 279 (1981)
- 7 F. Grein, S.D. Peyerimhoff and R.J. Buenker, Can. J. Phys. 62, 1928 (1984)
- 8 A.E. Douglas, Can. J. Phys. 59, 835 (1981)
- 9 T. Möller, B. Jordan, P. Gürtler, G. Zimmerer, D. Haaks, J. Le Calvé and M.C. Castex, Chem. Phys. 76, 295 (1983)
- 10 J. Jureta, S. Cvejanović, M. Kurepa and D. Cvejanović, Z. Phys. A304, 143 (1982)
- 11 D. Spence, R.H. Huebner, H. Tanaka, M.A. Dillon, and R.-G. Wang, J. Chem. Phys. 80, 2989 (1974)
- 12 L.C. Lee, M. Suto and K.Y. Tang, J. Chem. Phys. 84, 5277 (1986)
- 13 T. Ishiwata, I. Fujiwara and I. Tanaka, Chem. Phys. Lett. 89, 527 (1982)
- 14 T. Ishiwata, I. Fujiwara, T. Shinzawa and I. Tanaka, J. Chem. Phys. 79, 4779 (1983)
- 15 T. Ishiwata and I. Tanaka, Chem. Phys. Lett. 107, 434 (1984)
- 16 T. Ishiwata, A. Tokunaga and I. Tanaka, Chem. Phys. Lett. 112, 356 (1984)
- 17 T. Ishiwata, T. Shinzawa, T. Kusayanagi and I. Tanaka, J. Chem. Phys. 82, 1788 (1985)
- 18 T. Shinzawa, A. Tokunaga, T. Ishiwata and I. Tanaka, J. Chem. Phys. 83, 5407 (1985)
- 19 T. Noll, J. Kruppenbacher, K. Molter, J. Imschweiler and H. Schmoranzler, in Annual Report 1985 of BESSY (Berlin), p. 85; H. Schmoranzler, in Proc. 8th Internat. Conf. on Spectral Line Shapes, Williamsburg 1986 (in press)
- 20 H. Wilcke, W. Böhmer, R. Haensel and K. Schwentner, Nucl. Instr. Meth. 208, 59 (1983)
- 21 J. Le Calvé, M.C. Castex, D. Haaks, B. Jordan and G. Zimmerer, Il Nuovo Cim. 63B, 265 (1981)
- 22 P. Gürtler, E. Roick, G. Zimmerer and M. Pouey, Nucl. Instr. Meth. 208, 835 (1983)
- 23 T. Möller, P. Gürtler, E. Roick and G. Zimmerer, Nucl. Instr. Meth. A246, 461 (1986)
- 24 T. Möller and G. Zimmerer, Phys. Script. T17 (1987, in press)
- 25 R.S. Mulliken, J. Chem. Phys. 55, 309 (1971)
- 26 J. Tellinghuisen, Adv. in Chem. Phys. 60, 299 (1985)
- 27 F.H. Mies and P.S. Julienne, IEEE J. Quantum Electron. QE-15, 272 (1979)
- 28 H.M. Hulbert and J.O. Hirschfelder, J. Chem. Phys. 9, 61 (1941)
- 29 R.L. Jaffe, private communication
- 30 L.D. Landau, Phys. Z. Sowjetunion 1, 46 (1932)
C. Zener, Proc. Roy. Soc. A137, 696 (1932)
- 31 K. Dressler, Annals of the Israel Phys. Soc. 6, 141 (1983)
- 32 L.D. Landau and E.M. Lifschitz, Quantenmechanik (Akademie Verlag Berlin 1966)
- 33 T. Möller, Diploma thesis, University of Hamburg (1982) and Internal Report DESY-HASYLAB 82-07 (Oct. 1982), Hamburg
- 34 Y.C. Yu, Ph.D. thesis, Kansas State University, Manhattan, Kansas, 1984
- 35 S.D. Peyerimhoff, private communication
- 36 T. Ishiwata, A. Tokunaga, T. Shinzawa and I. Tanaka, J. Mol. Spectr. 108, 314 (1984)
- 37 A.R. Hoy, J. Mol. Spectr. 115, 232 (1986)
- 38 J. Tellinghuisen and D.K. Chakraborty, Chem. Phys. Lett. (in press)
- 39 T. Möller, B. Jordan, G. Zimmerer, D. Haaks, J. Le Calvé, and M.C. Castex, Z. Phys. D4, 73 (1986)
- 40 J. Wörmer, Diploma thesis, University of Hamburg (1986)

Figure Captions

Figure 1

Typical fluorescence spectra of Cl_2 following primary excitation of $1^1\Sigma_u^+$ (upper curve) and of $2^1\Sigma_u^+$. E_{ex} is the excitation energy. Band pass in fluorescence analysis 1 nm, in excitation .05 nm (upper curve) and .25 nm. Time window $\Delta t = 20$ ns, gas pressure $p = .1$ torr. The meanings of E_1 , E_2 , and E_3 are explained in the text.

Figure 2

Bound-bound fluorescence $1^1\Sigma_u^+ (v' = 39) \rightarrow X^1\Sigma_g^+ (v'')$, analysed with a band pass of .2 nm. Band pass in excitation .25 nm, gas pressure .4 torr, time window $\Delta t = 50$ ns. The transition energies terminating at $v'' = 0 \dots 11$ are indicated by bars.

Figure 3

Potential energy curves of the ground state [5] and of the $1^1\Sigma_u^+$ state (this work) of Cl_2 . The difference potential corresponding to an excitation energy E_0 is included (dotted curve). The meanings of E_1 , E_2 , and E_3 are explained in the text.

Figure 4

Comparison of the potential energy curve of the $1^1\Sigma_u^+$ state of Cl_2 obtained in this work (full curve) with the results of Möller et al. [9] (dotted curve), Peyerimhoff and Buenker [6] (quadratic dots), Jaffe [29] (crosses), and of Ishiwata et al. [14] (curve of the "γ-state"). The curve of the $2^1\Sigma_u^+$ state is a fit of the calculated points [6] (outer minimum) and of the spectroscopic data of [9] (inner minimum).

Figure 5

Comparison between the measured fluorescence curves of Cl_2 and a computer simulation of their bound-free parts. Experimental data: band pass of excitation .05 nm, of fluorescence analysis 1 nm, gas pressure .1 torr, time window 20 ns. The model calculation with the coarse and fine structure is described in the text.

Figure 6

Fluorescence excitation spectra of Cl_2 . Upper curve: the zero'th order light of the fluorescence monochromator. Lower curve: spectrally selected fluorescence ($\lambda = 200$ nm, band pass 4 nm). Gas pressure 0.1 torr (upper

curve) and 1 torr. Time window 20 ns. The excitation energies terminating at $v' = 32 \dots 40$ of $1^1\Sigma_u^+ (v') \leftarrow X^1\Sigma_g^+ (v'' = 0)$ ($^{35}\text{Cl}_2$) are indicated.

Figure 7

Ratio of bound-bound vs. bound-free fluorescence (each one integrated over the respective part of the fluorescence spectrum) as a function of the vibrational quanta of the emitting $1^1\Sigma_u^+$ state which have been excited selectively.

Figure 8

Comparison between measured and calculated bound-free fluorescence spectra of Cl_2 . The excitation energies, E_{ex} , and the vibrational quanta of the excited states are given (for details see text). Experimental conditions: band pass of excitation .25 nm, of fluorescence analysis 1 nm; gas pressure .1 torr; time window 20 ns (curves with $E_{\text{ex}} = 78019 \text{ cm}^{-1}$, 79443 cm^{-1} , 80024 cm^{-1} , and 86067 cm^{-1}); gas pressure 1 torr, other parameters as above ($E_{\text{ex}} = 81512 \text{ cm}^{-1}$). The curve with $E_{\text{ex}} = 73448 \text{ cm}^{-1}$ was obtained with a band pass of excitation .05 nm, and with a gas pressure .1 torr.

Figure 9

Schematic representation of the potential energy curves of the diabatic Rydberg and valence states and of the adiabatic states under discussion.

Figure 10

Plot of ΔE^3 (ΔE : splitting of the coarse structure of the bound-free fluorescence spectra) vs. the excitation energies (points). The full curve corresponds to the linear approximation according to Equ. (5). The dotted curve is an approximation including higher order terms (see text).

Figure 11

Fluorescence spectra of Cl_2 following primary excitation with lower photon energies (the excitation energies, E_{ex} , are given in the figure, band pass of fluorescence 1 nm, time window 20 ns). The band pass of excitation is 0.05 nm, the gas pressure is .1 torr (curves a), b)); 0.25 nm and 1 torr (curve c)); 0.25 nm and 10 torr (curves d) and e)).

Figure 12

Fluorescence of Cl_2 measured by Yu [34] (excitation with a Xe-lamp). The excitation energy and the gas pressure are given in the figure. The transitions terminating at $v'' = 37 \dots 49$ of $1^1\Sigma_u^+ (v' = 16) \leftarrow X^1\Sigma_g^+ (v'')$ are indicated by bars.

Figure 13

Potential energy curves of the lowest ion-pair states of Cl_2 with ungerade symmetry. The curves for the α - and the γ -state are Morse fits of the results of Ishiwata et al. [14]. The β -state curve is a harmonic oscillator fit of the results of Ref. 14. The dots represent ab initio calculations of $2^3\Pi_u$ [35]. The $1^1\Sigma_u^+$ potential energy curve is a result of this paper.

Appendix: Description of the $1^1\Sigma_u^+$ potential energy curve

It was tried to construct the $1^1\Sigma_u^+$ potential energy curve, $V(r)$, from two potential energy curves, which can be used as an approximation of the diabatic potential energy curves of $1^1\Sigma_u^+(\text{Val})$ and $1^1\Sigma_u^+(\text{Ryd})$. Two weight functions (f_1, f_2) are introduced in a way that in the center of the interaction the valence part merges into the Rydberg part (see also Fig. 9).

In the asymptotic limit the valence part, $\text{Val}(r)$, is described by the Coulomb law. However, approaching the minimum, an additional attraction correction has to be introduced. Therefore, a Rittner potential is not sufficient. A Morse-type correction was added to a Rittner potential. Concerning the Rydberg-type curve, $\text{Ryd}(r)$, a Morse potential can be used. $V(r)$ is given by

$$V(r) = f_1(r) \cdot \text{Val}(r) + f_2(r) \cdot \text{Ryd}(r) \quad (\text{A1})$$

with

$$\text{Val}(r) = -(Z/r) + E_1 + A[(1 - e^{-a(r-r_{eV})})^2 - 1] + Be^{-br} \quad (\text{A2})$$

and

$$\text{Ryd}(r) = C(1 - e^{-c(r-r_{eR})})^2 + T_{eR} \quad (\text{A3})$$

The weight functions are

$$f_1(r) = (e^{-\alpha(r-r_x-\Delta r)} + 1)^{-1} \quad (\text{A4})$$

$$f_2(r) = (e^{\alpha(r-r_x+\Delta r)} + 1)^{-1} \quad (\text{A5})$$

E_1 yields the correct asymptotic limit, Z determines the correct Coulomb potential for large r . The center of the interaction is at $r = r_x$. The steepness of the weight functions around the center of the interaction is described by α .

The numerical values of the constants are: $Z = 116645 \text{ cm}^{-1} \cdot \text{\AA}$; $E_1 = 108104 \text{ cm}^{-1}$; $A = 6500 \text{ cm}^{-1}$; $a = 1.04 \text{ \AA}^{-1}$; $r_{eV} = 2.7 \text{ \AA}$; $B = 9.59069 \cdot 10^5 \text{ cm}^{-1}$; $b = 1.84917 \text{ \AA}^{-1}$; $C = 20558 \text{ cm}^{-1}$; $c = 2.192 \text{ \AA}^{-1}$; $r_{eR} = 1.852 \text{ \AA}$; $T_{eR} = 73428 \text{ cm}^{-1}$; $r_x = 2.03 \text{ \AA}$; $\Delta r = 0.0058 \text{ \AA}$; $\alpha = 32$.

With the potential energy curves $V_{al}(r)$ and $R_{yd}(r)$ it is also possible to construct an approximative curve of the inner well of the adiabatic state $2^1\Sigma_u^+$ [40]. For this purpose, however, different weight functions are necessary.

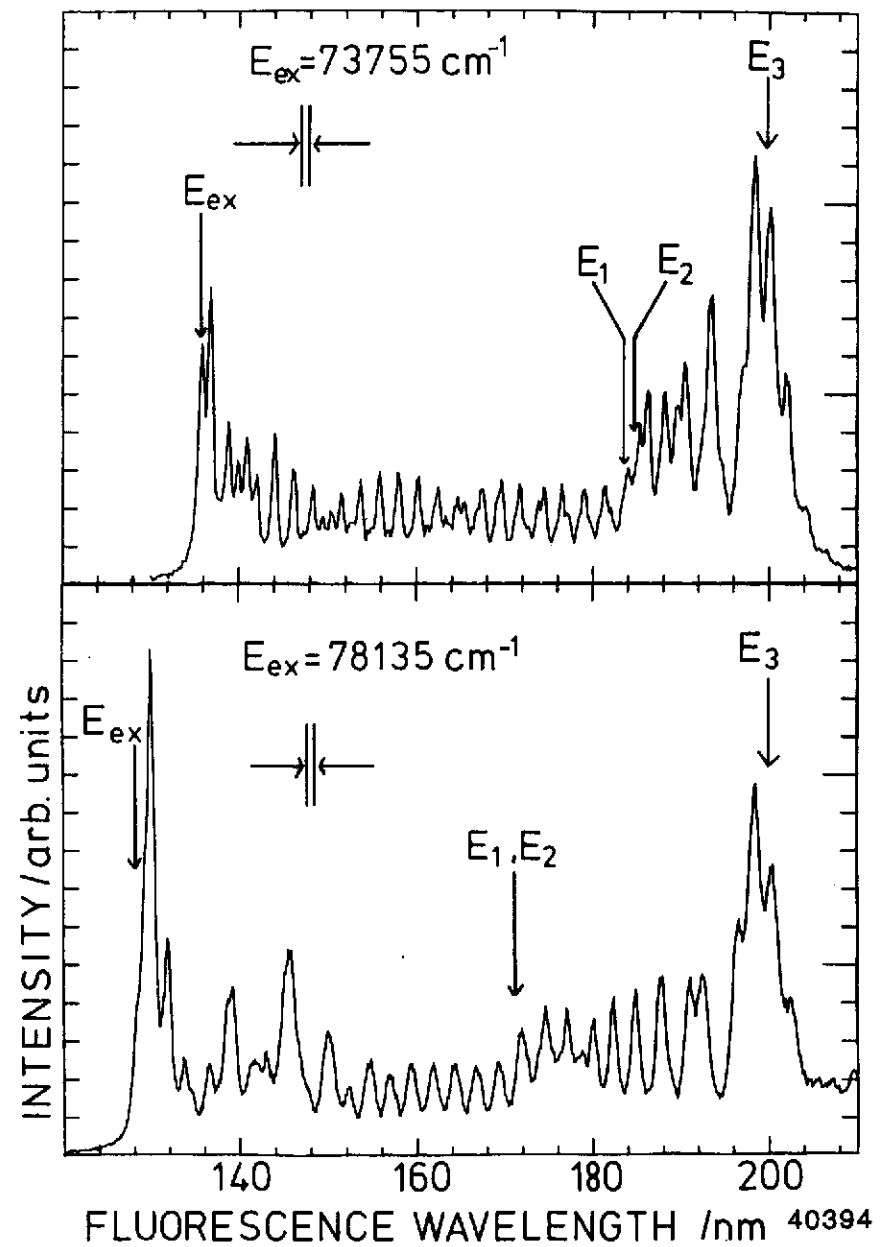
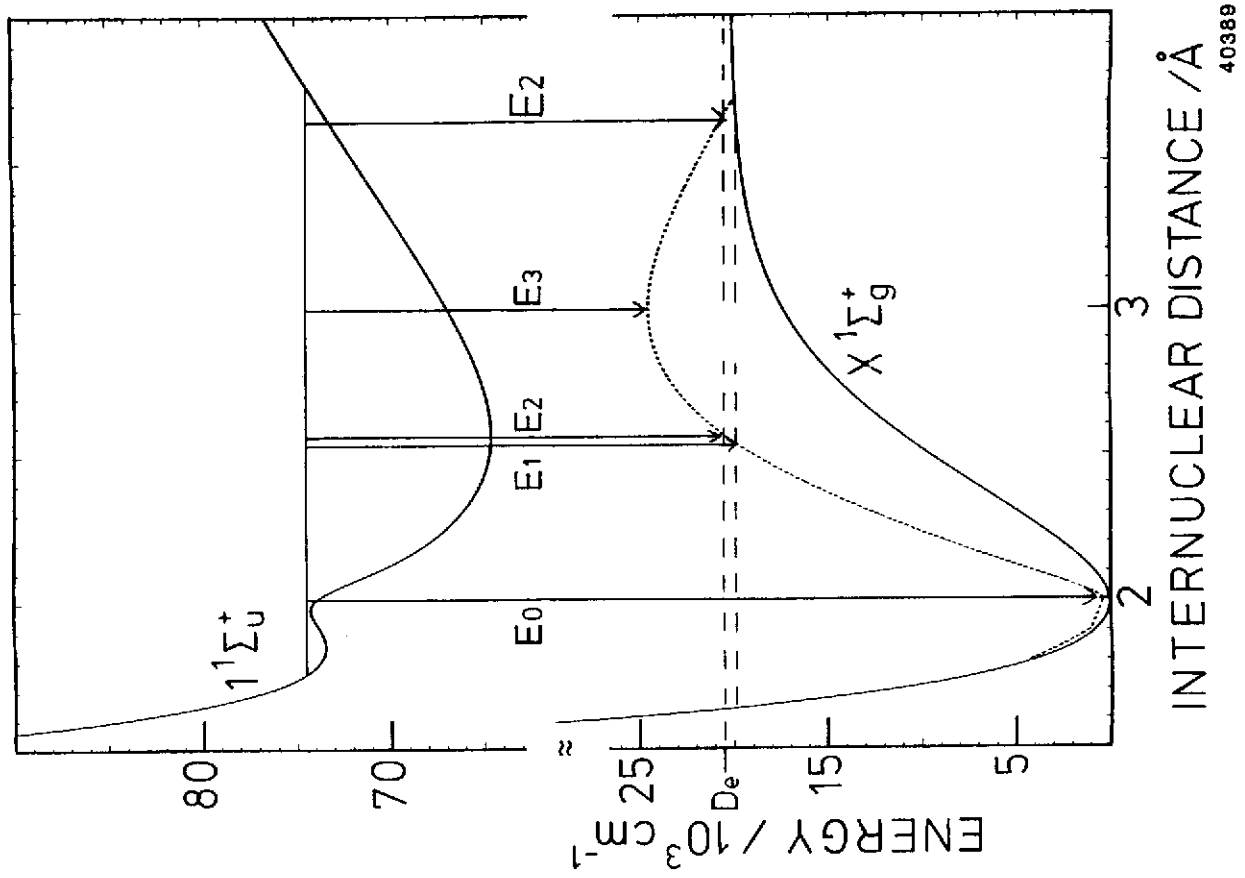


Fig. 1



40389

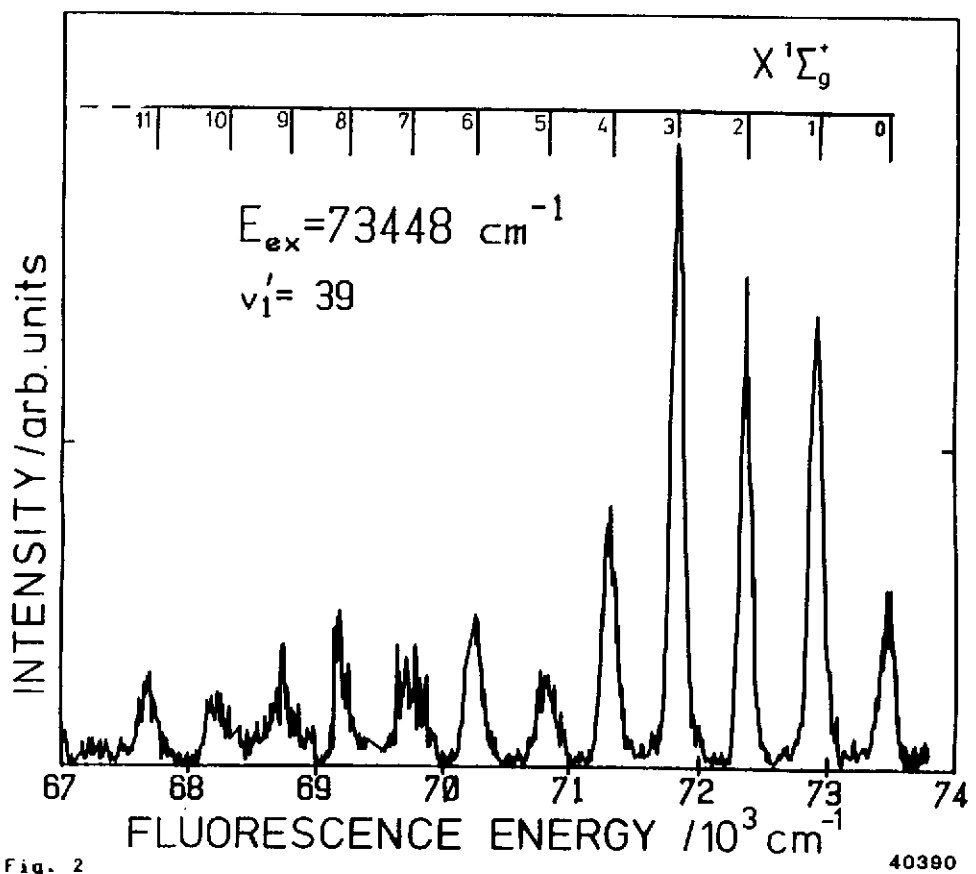
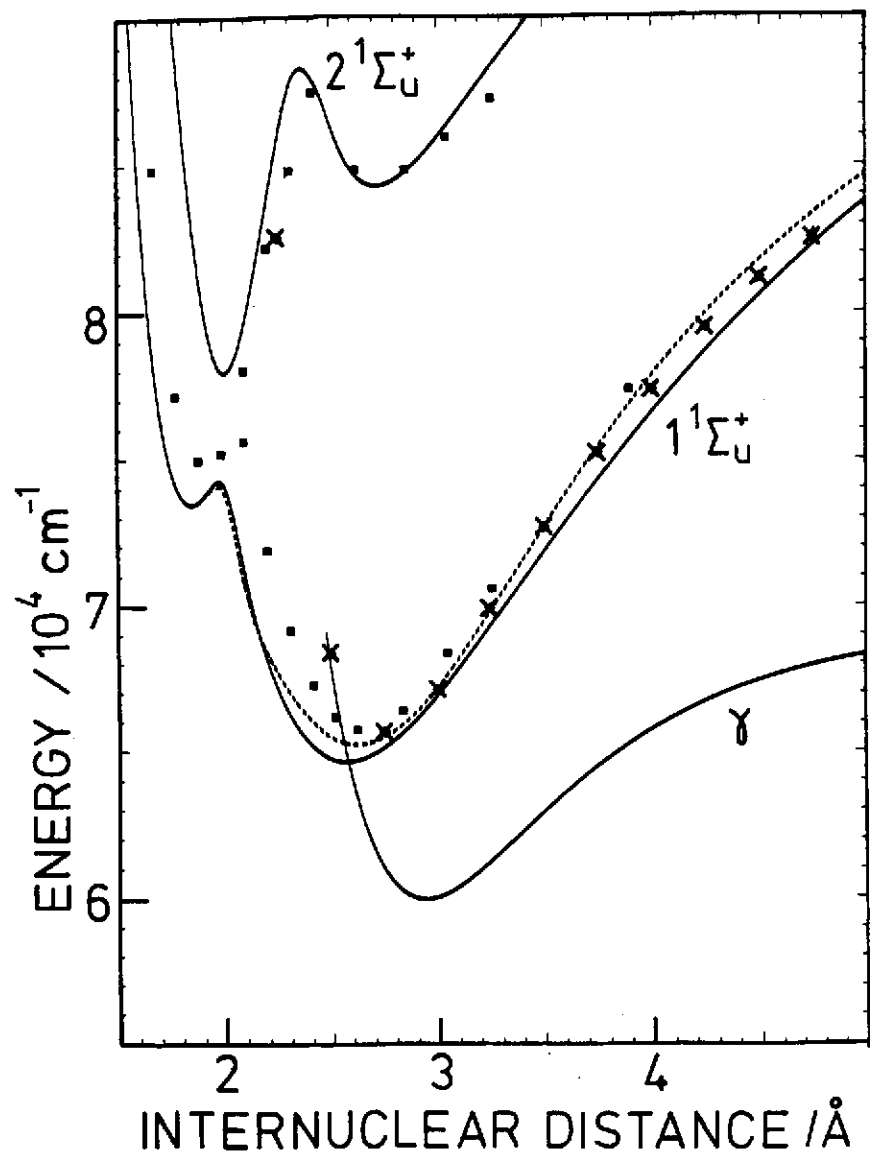


Fig. 2

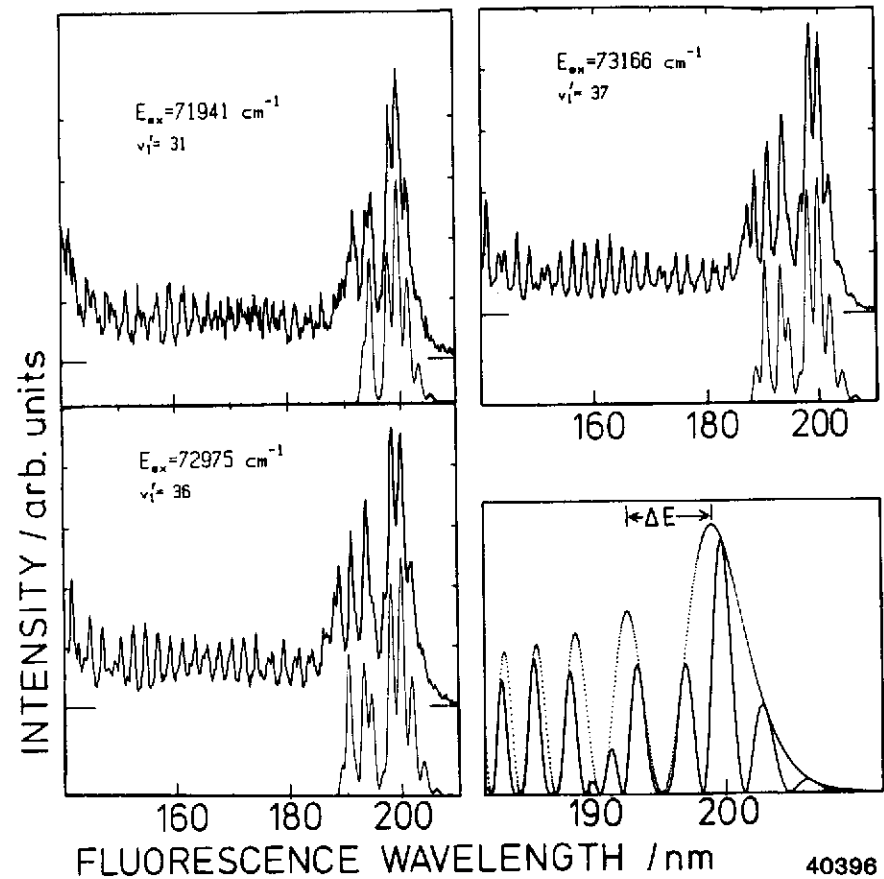
40390

Fig. 3



40391

Fig. 4



40396

Fig. 5

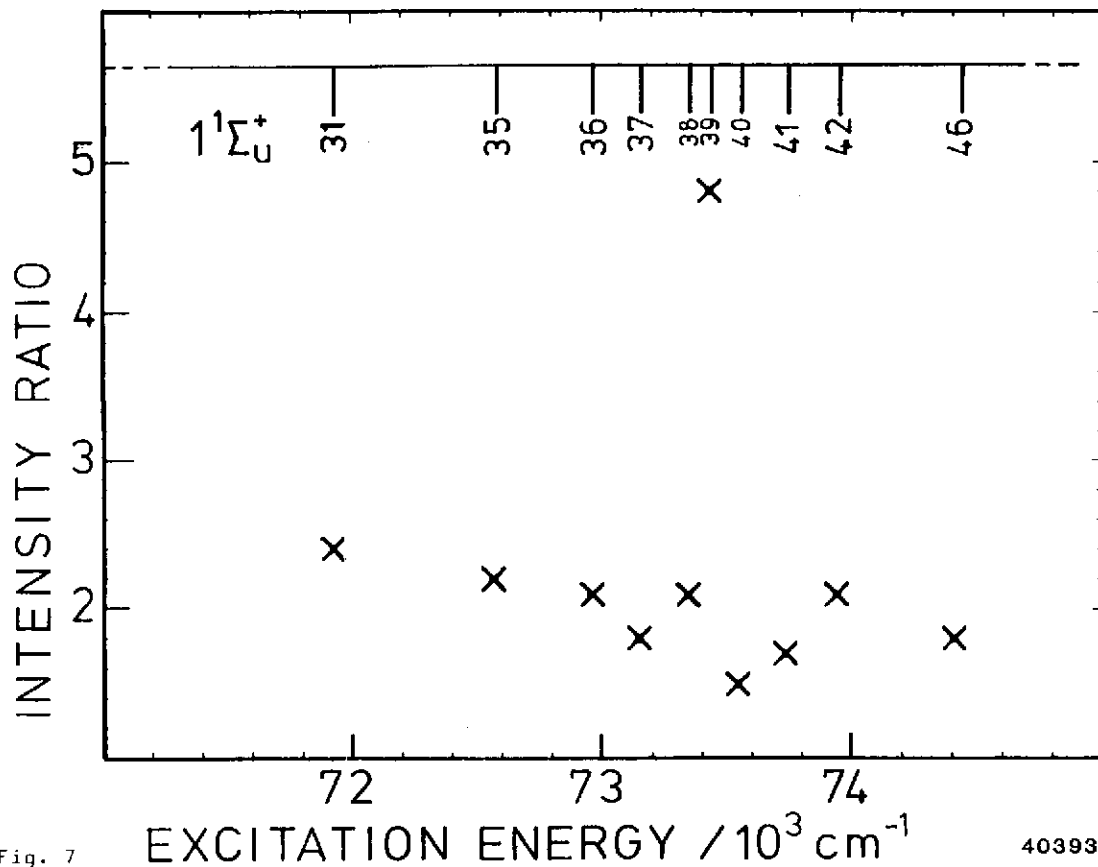


Fig. 7

40393

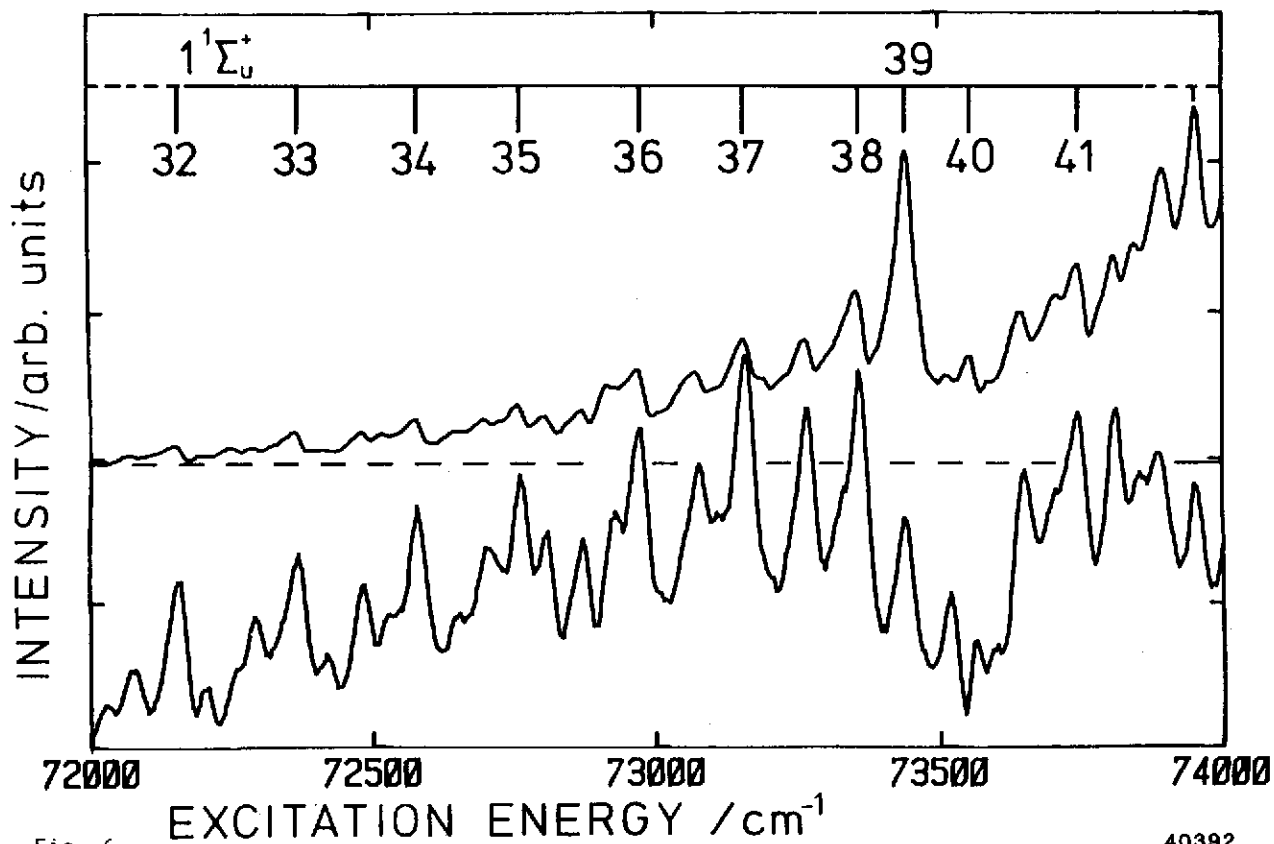


Fig. 6

40392

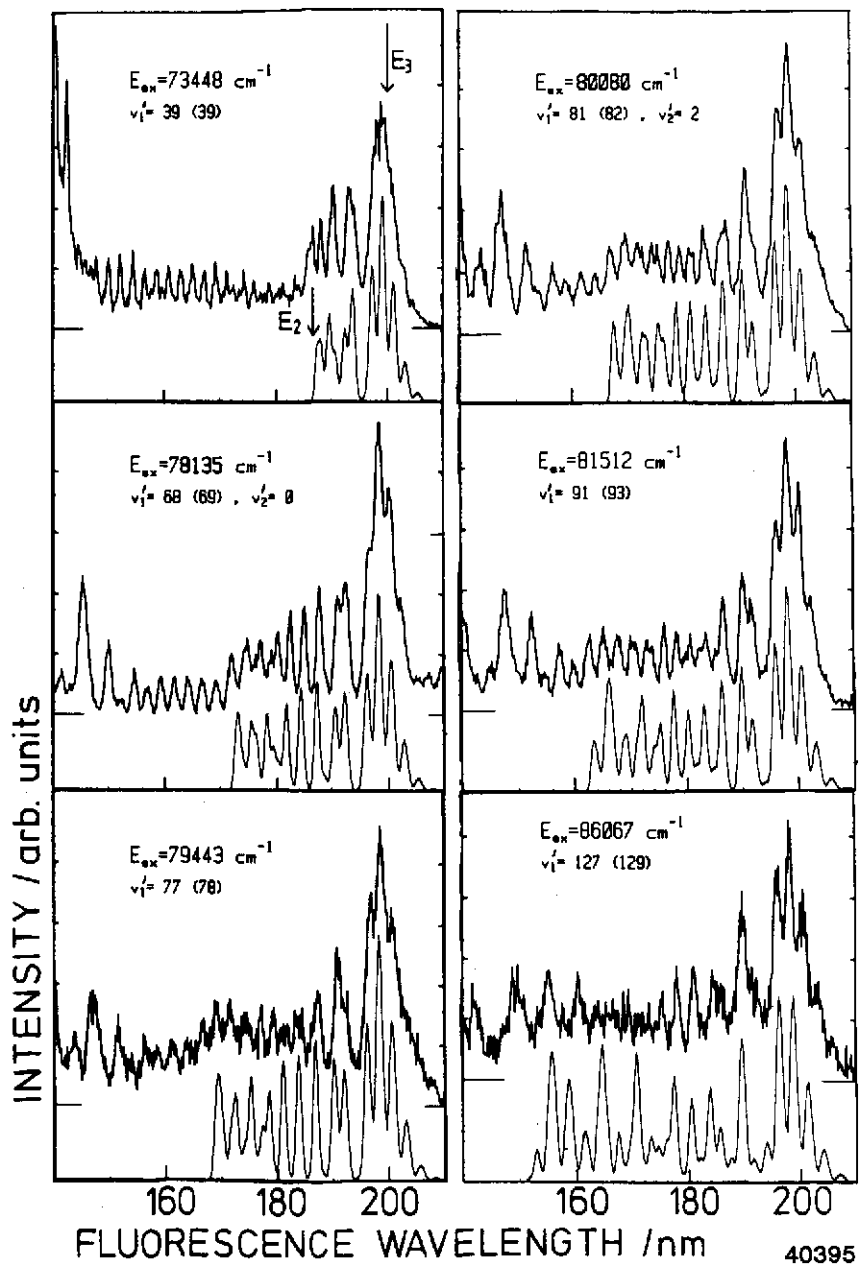


Fig. 8

FIG. 9

INTERNUCLEAR DISTANCE / Å

40558

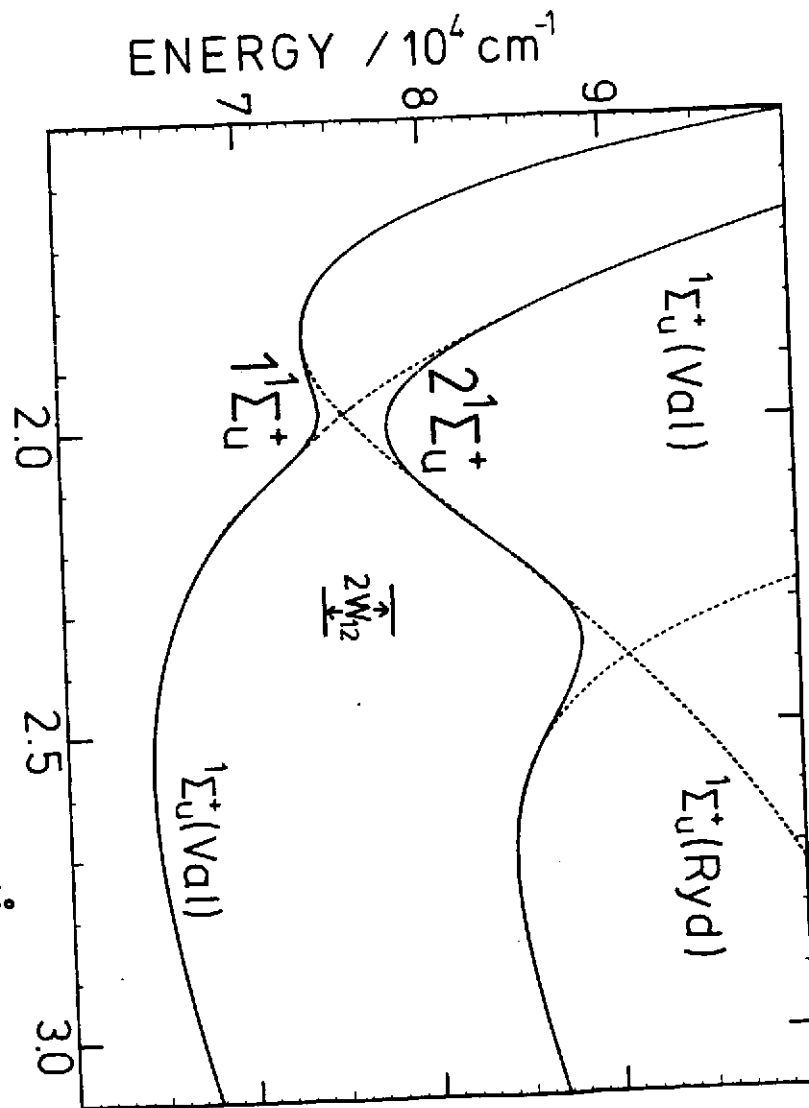
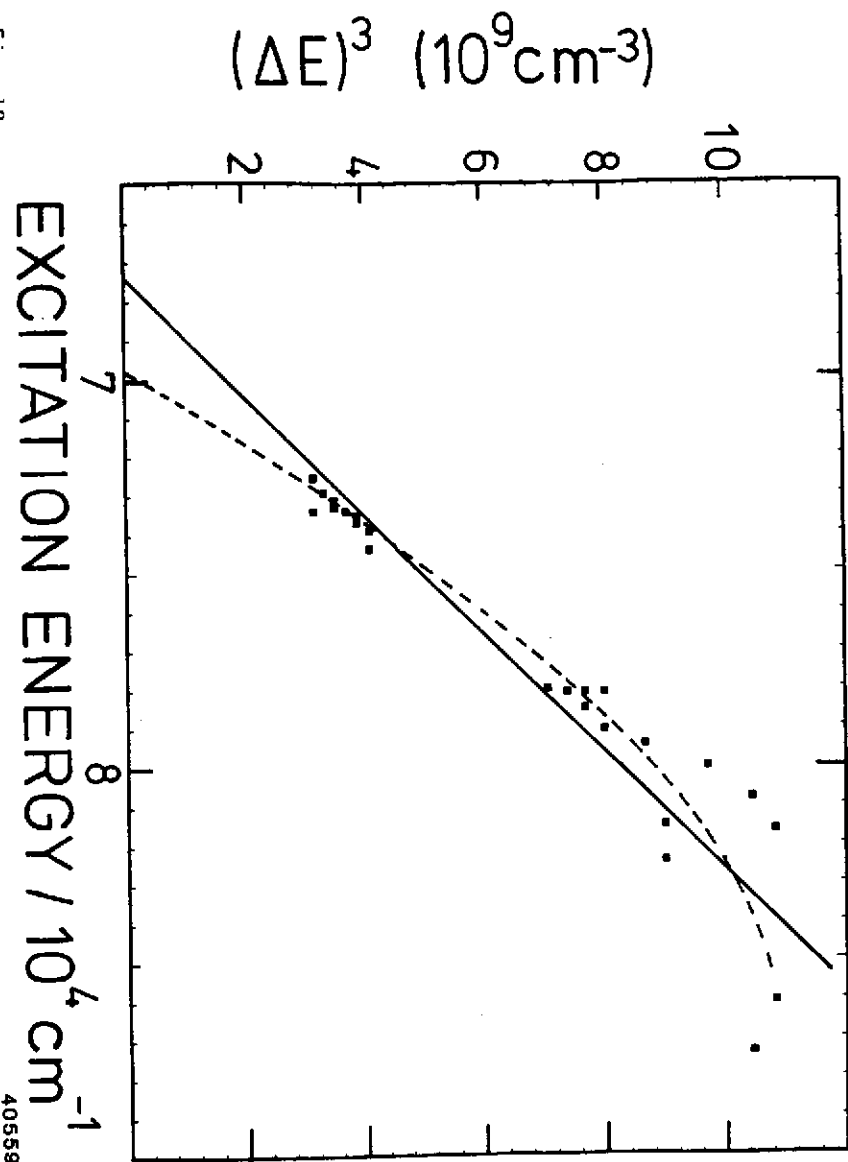
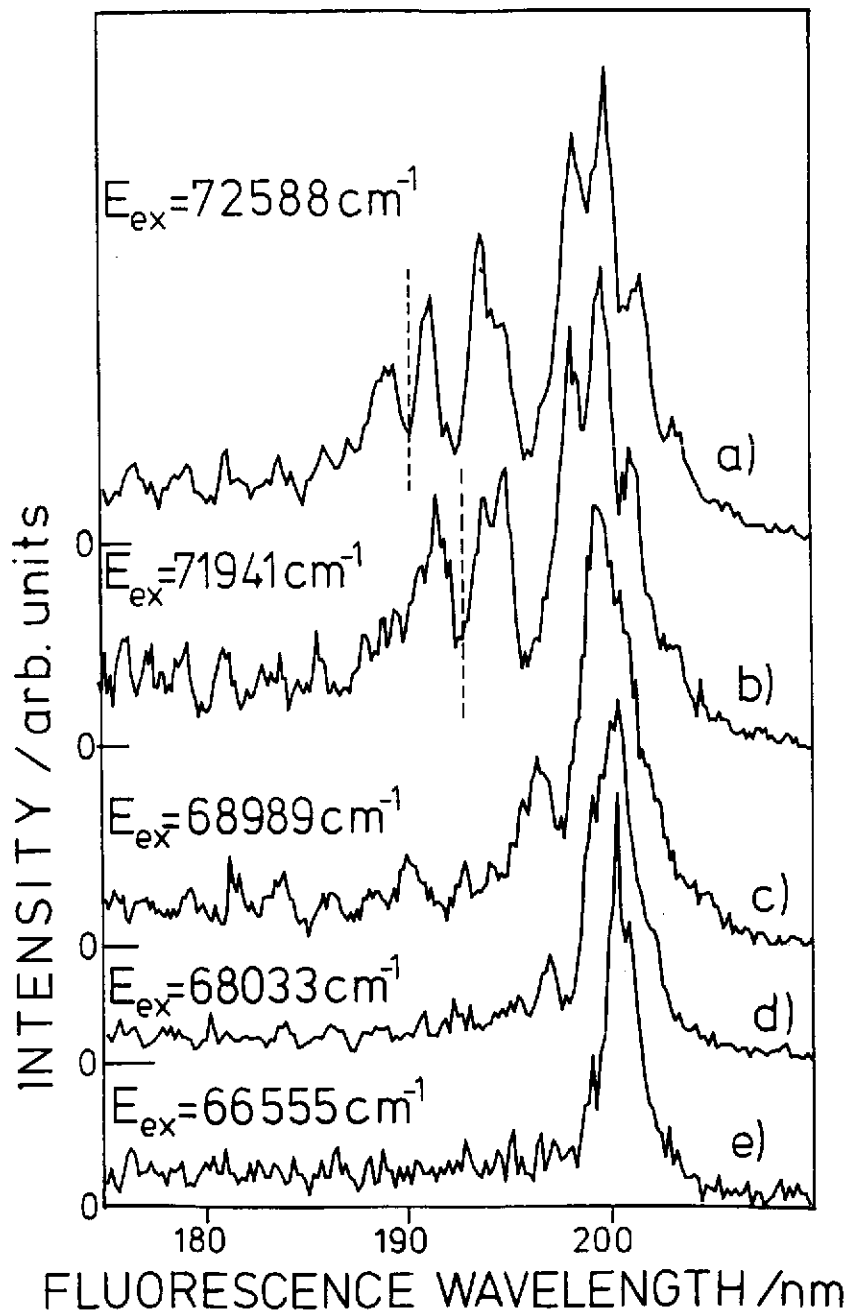


Fig. 10



40559



40556

Fig. 11

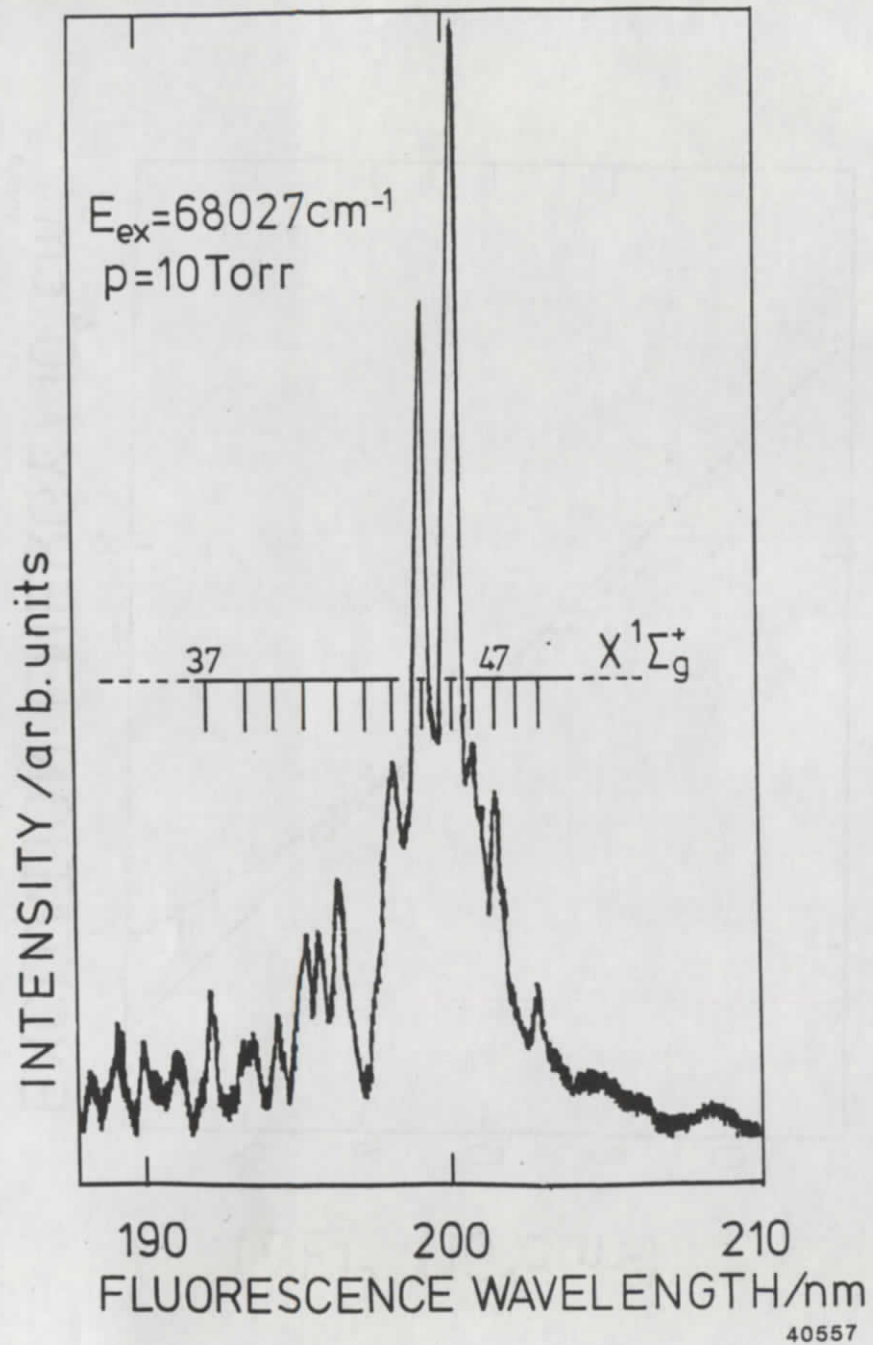


Fig. 12

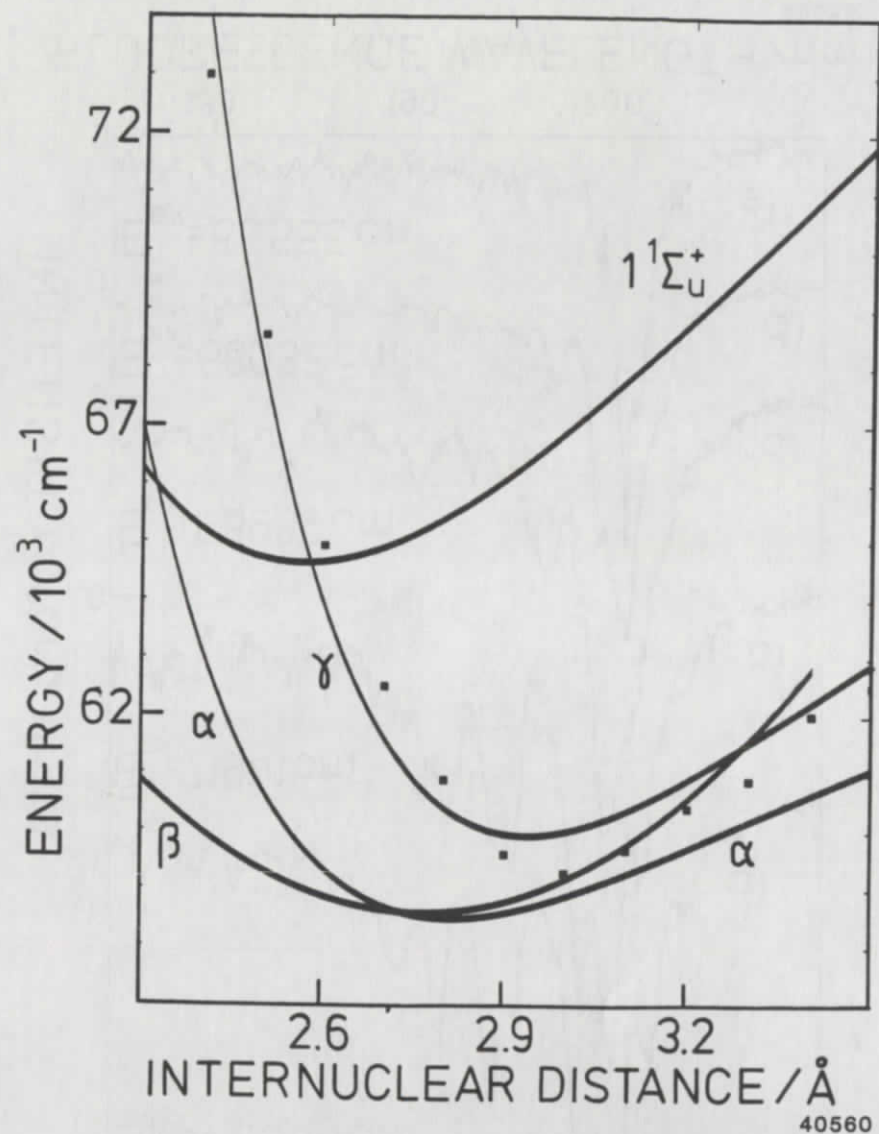


Fig. 13